Multi-azimuth prestack time migration for anisotropic weakly heterogeneous media

Walter Söllner[1], Ilya Tsvankin[2], & Eduardo Filpo Ferreira da Silva[3]
[1] *Petroleum Geo-Services, Lysaker, Norway*
[2] *Center for Wave Phenomena, Colorado School of Mines, Golden, CO*
[3] *Petrobras, Rio de Janeiro, Brazil*

ABSTRACT

Conventional prestack time-migration velocity analysis is designed to estimate diffraction time functions in a fixed azimuthal direction from narrow-azimuth reflection data. Therefore, it can build accurate 3D migration operators only if the subsurface is isotropic (or azimuthally isotropic) and laterally homogeneous. Here, we extend time-migration methodology to multi-azimuth or wide-azimuth data from azimuthally anisotropic, weakly heterogeneous media.
We derive the azimuthally varying diffraction time function from the most general form of Hamilton's principal equation and apply a Taylor series expansion to the traveltime in the vicinity of the image ray. This approach helps to relate the Taylor series coefficients to the corresponding multi-azimuth imaging parameters. The second-order coefficients, which define the "migration-velocity ellipse," are obtained from time-migration velocity analysis in at least three distinct azimuthal directions. Our multi-azimuth prestack time migration (MAPSTM) solves the mismatch problem that occurs in conventional processing when the same depth point creates different time images in different azimuths. The algorithm is successfully tested on synthetic data for a horizontally layered azimuthally anisotropic model and an isotropic medium with a dipping interface.

Key words: time migration, velocity analysis, azimuthal anisotropy, NMO ellipse, image ray, multi-azimuth surveys.

1 INTRODUCTION

Conventional prestack time-migration operators are derived from analytic diffraction time functions. The diffraction times for any source and receiver position are defined solely by a single average velocity (i.e., the RMS velocity) at the image point instead of the true velocity field above the reflector. The time-migration velocity is obtained by focusing analyses on prestack time-migrated gathers. This approach generally proved to be robust for narrow-azimuth 2D and 3D seismic data, particularly when the subsurface is not structurally complex.

However, the limitations of the conventional time-migration methodology have become obvious with the advent of multi-azimuth and wide-azimuth seismic surveys. The most important advantages of multi-azimuth data acquisition are improved noise suppression, multiple attenuation and target illumination (Manning *et al.*, 2007); wide azimuthal coverage can also help in anisotropic parameter estimation. As discussed by Keggin *et al.* (2007), one of the the biggest problems in conventional processing of multi-azimuth data is that summation of signals acquired at different azimuths does not account for traveltime differences due to azimuthal anisotropy and/or lateral velocity variation.

Time imaging for orthorhombic symmetry, which adequately describes fracture-induced azimuthal anisotropy, is discussed by Grechka & Tsvankin (1999). They show that all P-wave time processing steps (normal-moveout and dip-moveout corrections, prestack and poststack time migration) for a laterally homogeneous orthorhombic medium above a dipping

reflector are controlled by the orientation of the vertical symmetry planes, the symmetry-plane normal-moveout (NMO) velocities from a horizontal interface $[V_{\rm nmo}^{(1,2)}]$ and three anellipticity parameters $\left[\eta^{(1,2,3)}\right]$. The velocities $V_{\rm nmo}^{(1,2)}$ and the symmetry-plane azimuth can be found using the NMO ellipse (Grechka & Tsvankin, 1998) of a horizontal event. Then the NMO ellipse from a dipping reflector is used to estimate the parameters $\eta^{(1,2,3)}$ responsible for the dip-dependence of normal moveout. Alternatively, it is possible to obtain $\eta^{(1,2,3)}$ from azimuthally varying nonhyperbolic moveout in a horizontal orthorhombic layer (Vasconcelos & Tsvankin, 2006).

Note that the simpler HTI (transversely isotropic with a horizontal symmetry axis) medium represents a special case of orthorhombic symmetry. Therefore, the time-migration operator in azimuthally anisotropic media can be built using solely P-wave reflection traveltimes. This approach represents a generalization of the widely used time-imaging methodology for vertical transverse isotropy (VTI) based on the Alkhalifah-Tsvankin (1995) parameter η (Tsvankin, 2005).

A time-migration algorithm that takes azimuthal velocity variation into account is presented by Kappius in Grechka *et al.* (2006). The NMO ellipse is reconstructed from azimuthal moveout analysis or iteratively applied azimuthal prestack time migration that preserves offset and azimuth information. The author mentions the ambiguity in the azimuthal correction caused by dipping structures and suggests to separate the contributions of azimuthal anisotropy and dip during an iterative process of velocity analysis and imaging. Preservation of the offset (source-receiver) vector information during prestack time migration of wide-azimuth data is further exploited by Calvert *et al.* (2008).

Azimuthally-dependent velocities estimated from focusing analyses are used in time migration to handle the influence of structure in laterally heterogeneous media (Söllner & Andersen, 2005). The authors employ the surface-to-surface paraxial ray theory (Bortfeld, 1989; Hubral *et al.*, 1992) to introduce kinematic time migration that operates with azimuthally-varying NMO velocities and zero-offset traveltime slopes, as well as the corresponding demigration based on azimuthally-varying time-migration velocities and slopes.

Here, starting from the generalized surface-to-surface paraxial matrices (Moser & Červený, 2007), we develop a multi-azimuth prestack time-migration algorithm for arbitrarily anisotropic, weakly heterogeneous media. Hamilton's point characteristic for transmitted rays helps to link the surface-to-surface paraxial matrices to azimuthally varying time-migration velocities and derive the time-migration operator. Focusing analysis for the full range of available azimuths is used to estimate the time-migration velocities, which are shown to be generally different from NMO velocities. The migration operator can still be developed from the NMO ellipse, but only by including additional information provided by zero-offset time slopes.

2 METHODOLOGY

2.1 Surface-to-surface paraxial matrices

We consider a model comprised of a stack of heterogeneous, anisotropic layers separated by smooth interfaces (Bortfeld, 1989; Hubral *et al.*, 1992; Moser & Červený, 2007). Smoothness here means that each interface can be locally represented by second-order polynomials. The sources and receivers are located at the top interface called the anterior (earth's) surface. In the marine environment, this surface can be considered flat. The bottom interface, called the posterior surface, represents the reflector. A selected ("central") ray travels from the anterior to the posterior surface. The central ray intersects the anterior surface at the origin (point P_0) of a Cartesian (x, y, z) coordinate system and the posterior surface at the origin (P_0') of another Cartesian (x', y', z') coordinate system.

The plane tangent to the anterior surface at P_0 is taken as the $[x, y]$ plane of the (x, y, z) coordinate system; the direction of the x- and y-axes in this plane is arbitrary. The central ray can be described by four three-component vectors: the initial position vector $\tilde{\mathbf{x}}_0$, the initial slowness vector $\tilde{\mathbf{p}}_0$, the final position vector $\tilde{\mathbf{x}'}_0$, and the final slowness vector $\tilde{\mathbf{p}'}_0$.

Likewise, an arbitrary ray propagating from point P at the anterior surface may be described by the initial position ($\tilde{\mathbf{x}}$) and slowness ($\tilde{\mathbf{p}}$) vectors. The corresponding final vectors ($\tilde{\mathbf{x}'}$ and $\tilde{\mathbf{p}'}$) at the posterior surface are measured in the (x', y', z') Cartesian coordinate system. The two-dimensional vectors $\mathbf{x}$, $\mathbf{p}$, $\mathbf{x}'$, and $\mathbf{p}'$ are obtained by projecting the three-dimensional position and slowness vectors onto the initial and final tangent planes, respectively. Each component of the vectors $\mathbf{x}'$ and $\mathbf{p}'$ is a complicated function of the four components of the initial vectors: $\mathbf{x}'=\mathbf{x}'(\mathbf{x},\mathbf{p})$ and $\mathbf{p}'=\mathbf{p}'(\mathbf{x},\mathbf{p})$. Therefore, it is convenient to introduce first-order (paraxial) approximations. These approximations for $\mathbf{x}'$ and $\mathbf{p}'$ correspond to second-order approximations of the traveltime function t and are valid for relatively small magnitudes of the vectors $\mathbf{x}$, $\mathbf{p}-\mathbf{p_0}$, $\mathbf{x}'$, and $\mathbf{p}'-\mathbf{p_0'}$ (i.e., in the vicinity of the central ray). Hereafter, the magnitudes of all vectors are obtained within the framework of the first-order (paraxial) approximation.

The central ray and all paraxial rays in its vicinity can be described by the 4×4 matrix,

$$T(P_0', P_0) \equiv \begin{pmatrix} \mathbf{A}_0 & \mathbf{B}_0 \\ \mathbf{C}_0 & \mathbf{D}_0 \end{pmatrix}, \qquad (1)$$

where $\mathbf{A}_0$, $\mathbf{B}_0$, $\mathbf{C}_0$, and $\mathbf{D}_0$ are 2×2 surface-to-surface

paraxial matrices (Moser & Červený, 2007), which describe the transmission of the central ray between the anterior and posterior surfaces:

$$\begin{pmatrix} \mathbf{x}' \\ \mathbf{p}' - \mathbf{p}'_0 \end{pmatrix} = \begin{pmatrix} \mathbf{A}_0 & \mathbf{B}_0 \\ \mathbf{C}_0 & \mathbf{D}_0 \end{pmatrix} \begin{pmatrix} \mathbf{x} \\ \mathbf{p} - \mathbf{p}_0 \end{pmatrix}. \tag{2}$$

Given the deviations from the central ray in the initial position ($\mathbf{x}$) and slowness ($\mathbf{p} - \mathbf{p_0}$) vectors, equation 2 yields the corresponding vectors at the posterior surface, if the matrices $\mathbf{A}_0$, $\mathbf{B}_0$, $\mathbf{C}_0$, and $\mathbf{D}_0$ are known. The surface-to-surface paraxial matrix $\mathbf{T}$ can also be computed from the paraxial ray propagator matrix using surface transformation matrices (Hubral *et al.*, 1992; Červený, 2001; Moser & Červený, 2007).

Assuming the existence of the inverse matrix $\mathbf{B}_0^{-1}$, equation 2 can be rewritten after simple algebraic operations as

$$\mathbf{p} = \mathbf{p}_0 + \mathbf{B}_0^{-1}\,\mathbf{x}' - \mathbf{B}_0^{-1}\mathbf{A}_0\,\mathbf{x}\,, \tag{3}$$

and

$$\mathbf{p}' = \mathbf{p}'_0 + \mathbf{C}_0\,\mathbf{x} - \mathbf{D}_0\,\mathbf{B}_0^{-1}\mathbf{A}_0\,\mathbf{x} + \mathbf{D}_0\,\mathbf{B}_0^{-1}\mathbf{x}'. \tag{4}$$

Therefore, the initial and final slowness vectors of any transmitted ray in the vicinity of the central ray can be computed from equations 3 and 4, respectively.

2.2 Traveltime of transmitted events

The traveltime difference between the central ray and a ray displaced at the anterior surface by $d\tilde{\mathbf{x}}$ and at the posterior surface by $d\tilde{\mathbf{x}}'$ can be found from Hamilton's principal equation as the total differential,

$$dt(\tilde{\mathbf{x}}, \tilde{\mathbf{x}}') = \tilde{\mathbf{p}}' \cdot d\tilde{\mathbf{x}}' - \tilde{\mathbf{p}} \cdot d\tilde{\mathbf{x}}\,. \tag{5}$$

Hamilton's equation was originally derived from general variational principles. For example, the proof of equation 5 for anisotropic media in Buchdahl (1970) is based on Fermat's principle. The partial derivatives ($\tilde{\mathbf{p}}'$ and $-\tilde{\mathbf{p}}$) of the total differential dt in equation 5 lead to the fundamental relationship between phase and group velocity for arbitrarily anisotropic media. Within the framework of our approximation, it is possible to replace the three-component vectors in equation 5 by their two-component counterparts (Bortfeld, 1989):

$$dt(\mathbf{x}, \mathbf{x}') = \mathbf{p}' \cdot d\mathbf{x}' - \mathbf{p} \cdot d\mathbf{x}\,. \tag{6}$$

Equation 6 preserves the general form of Hamilton's equation for the two-component position and slowness vectors.

Substituting equations 3 and 4 into equation 6 and integrating the resulting expression, we obtain:

$$t(\mathbf{x}, \mathbf{x}') = t_0 - \mathbf{p}_0 \cdot \mathbf{x} + \mathbf{p}'_0 \cdot \mathbf{x}' + \frac{1}{2}\mathbf{x}' \cdot \mathbf{D}_0\,\mathbf{B}_0^{-1}\mathbf{x}'$$

$$+ \frac{1}{2}\mathbf{x} \cdot \mathbf{B}_0^{-1}\mathbf{A}_0\,\mathbf{x} - \mathbf{x} \cdot \mathbf{B}_0^{-1}\,\mathbf{x}'\,; \tag{7}$$

t_0 is the exact one-way traveltime along the central ray. Equation 7, also known as Hamilton's point characteristic, yields the traveltimes of paraxial rays transmitted through an anisotropic heterogeneous medium between the anterior ($\mathbf{x}$) and posterior ($\mathbf{x}'$) surfaces. If known, the special form of Hamilton's point characteristic allows one to determine the complete seismic system. This property is very important for model parameter estimation.

2.3 Multi-azimuth prestack time migration

Time migration moves a weighted sum of the wavefield amplitudes measured at the diffraction time surface to the two-way traveltimes at the emerging point of the image ray. An image ray is a transmitted ray that originates at the surface with the slowness vector parallel to the surface normal and ends at the reflection point (Hubral & Krey, 1980). The diffraction time surface is obtained as the ensemble of the transmitted times from all source-receiver combinations to the reflection point. This type of migration is also called "diffraction stack" or "Kirchhoff-type migration."

The weighting functions are commonly applied to preserve the amplitude behavior of reflected waves, or in some cases even to compensate the amplitude for losses caused by geometrical spreading (Schleicher *et al.*, 2007). For example, simplified versions of such weights valid for horizontally layered media are often applied in time migration and are considered as known here.

To define the migration operator, we still need to obtain the diffraction time function of a hypothetical diffractor at the reflection point, the associated image ray and the two-way traveltime along that ray. Since the reflection point is generally unknown, neither traveltime can be found. To overcome this difficulty, we reformulate the problem by starting from the migrated volume. The amplitude at each time sample is considered to belong to a time image point built by stacking along the diffraction times of a diffractor at the endpoint of the image ray. If no reflector was found at the endpoint of the image ray, the amplitude of the corresponding time image sample is expected to vanish. A different approach that leads (theoretically) to the same migration result operates in the vicinity of the normal ray (see Appendix A).

We consider an arbitrary image ray (coveniently treated as the central ray) and build the diffraction time function for every time sample. Parameters related to this central ray will be denoted by the subscript "I." For example, the traveltime of the ray that connects the receiver $\mathbf{x}_r$ and the diffraction point $\mathbf{x}'$ at the reflector is obtained from Hamilton's point characteristic for transmitted rays (equation 7) by employing the image ray condition $\mathbf{p}_I = \mathbf{0}$ (Bortfeld, 1989; Hubral *et al.*,

1992; Moser & Červený, 2007):

$$t_r(\mathbf{x}_r,\mathbf{x}') = t_I + \mathbf{p'}_I\cdot\mathbf{x}' + \frac{1}{2}\mathbf{x}'\cdot\mathbf{D}_I\,\mathbf{B}_I^{-1}\mathbf{x}' + \frac{1}{2}\mathbf{x}_r\cdot\mathbf{B}_I^{-1}\mathbf{A}_I\,\mathbf{x}_r - \mathbf{x}_r\cdot\mathbf{B}_I^{-1}\,\mathbf{x}', \quad (8)$$

where t_I is the traveltime of the image ray, and $\mathbf{A}_I$, $\mathbf{B}_I$, $\mathbf{C}_I$, and $\mathbf{D}_I$ (see above) are the surface-to-surface paraxial matrices along the image ray (Moser & Červený, 2007).

If the diffraction point coincides with the endpoint of the image ray, all terms containing $\mathbf{x}'$ in equation 8 vanish (i.e., the dependence on the primed coordinates is eliminated). Hence, the hyperbolic approximation for the traveltimes of rays transmitted from any receiver position to the hypothetical diffraction point at the endpoint of the image ray simplifies to

$$t_r^2(\mathbf{x}_r,\mathbf{x}') = t_I^2 + t_I\,\mathbf{x}_r\cdot\mathbf{B}_I^{-1}\mathbf{A}_I\,\mathbf{x}_r. \quad (9)$$

Using equation 9 and an equivalent expression for the ray transmitted from the source position, the needed traveltimes may be calculated through the paraxial matrix combination $\mathbf{B}_I^{-1}\mathbf{A}_I$ by performing dynamic ray tracing along the image ray. Although it would be attractive to build the complete migration operator by tracing only the central ray, it is not feasible in most practical applications because the depth-domain velocity model is seldom known at the stage of time imaging.

Next, we take advantage of the fact that the diffraction time function in equation 9 depends only on the receiver coordinates at the anterior surface. Further, the 2×2 surface-to-surface matrix combination includes the "global" parameters of the seismic system (around a given central ray), which may be estimated by data search. The receiver position vector in equation 9 can be expressed through the azimuthal angle ϕ (measured counterclockwise from the x-axis) and the distance d_r between the image ray and receiver position:

$$t_r^2(\mathbf{x}_r,\mathbf{x}') = t_I^2 + d_r^2/V_{TM}^2(\phi), \quad (10)$$

with

$$V_{TM}^{-2}(\phi) \equiv t_I\,(U_{11}^I\,\cos^2\phi + 2U_{12}^I\,\cos\phi\sin\phi + U_{22}^I\,\sin^2\phi)\,. \quad (11)$$

$V_{TM}(\phi)$ is the time-migration velocity defined by the three independent "global" parameters (U_{11}^I, U_{12}^I, and U_{22}^I) of the symmetric matrix combination $\mathbf{B}_I^{-1}\mathbf{A}_I$. (The symmetry of $\mathbf{B}_I^{-1}\mathbf{A}_I$ is easily proved by building second order partial derivatives with respect to the coordinates in 9 and using the property that the order of differentiation is interchangeable.) Equations 10 and 11 are similar to the equation of the NMO ellipse in common-midpoint geometry derived by Grechka & Tsvankin (1998). A major difference between these two formulations is related to the definition of azimuth. While the azimuthal angle in the NMO formula is a data acquisition parameter (i.e., the direction of a source-receiver pair), ϕ in equations 10 and 11 is defined as the azimuth of the receiver position vector (i.e., the vector from the image ray to the receiver position) which generally deviates from the source-receiver direction (see Appendix A).

Equation 11, which represents the 3D velocity ellipse for time migration in heterogeneous anisotropic media, relates the three unknown parameters U_{11}^I, U_{12}^I, and U_{22}^I of Hamilton's point characteristic to the azimuthally varying time-migration velocity. Equations 10 and 11 can be applied to rays between the source and the diffraction point by substituting the distance to the source position, d_S, and the corresponding azimuthal angle γ. The diffraction time function for multi-azimuth 3D prestack time migration is obtained by adding the traveltimes for both legs of the reflected ray:

$$T_{TM} = t_r + t_s = \sqrt{t_I^2 + d_r^2/V_{TM}^2(\phi)} + \sqrt{t_I^2 + d_s^2/V_{TM}^2(\gamma)}. \quad (12)$$

Thus, the velocity ellipse and the time-migration operator are defined by three independent parameters, which can be estimated by time-migration velocity analysis in at least three distinct azimuthal directions. In practice, azimuthally-varying migration velocities are obtained from time-image gathers computed in regular surface intervals, which makes it possible to build the migration operator without knowledge of the medium parameters. Figure 1 shows the slice of a multi-azimuth time-migration operator for zero offset; there is a 20% difference between the migration velocities in the principal directions.

The method outlined here is designed to solve the mismatch problem that occurs in time migration of multi-azimuth data (i.e., when the same depth point creates different time images in different azimuthal directions). It is devised for weakly heterogeneous media of arbitrary symmetry and can be applied prior to anisotropic parameter estimation. The accuracy, however, is limited by the second-order approximation of the diffraction time function valid for small and moderate offsets. In contrast, the time-migration approach described by Grechka & Tsvankin (1999) for orthorhombic media does not rely on traveltime approximations but requires knowledge of the P-wave time-processing parameters (the azimuth of the vertical symmetry planes, the symmetry-plane NMO velocities $V_{\rm nmo}^{(1,2)}$, and the anellipticity parameters $\eta^{(1,2,3)}$).

3 SYNTHETIC TESTS

Conventional time migration leads to a mismatch of time-migrated events, if the velocity model is either laterally heterogeneous or azimuthally anisotropic. First, we illustrate migration errors caused by lateral heterogeneity by performing a test for an isotropic model with

an intermediate plane dipping interface (Figure 2). The synthetic volume included two 3D data sets with the acquisition azimuths in the dip and strike directions of the interface. Conventional prestack time migration including common-image-gather (CIG) velocity analysis was applied to each data set separately. Figure 3 shows image gathers for the horizontal reflector beneath the dipping interface computed in the dip and strike directions. Although the gathers obtained with the best-fit velocity in each direction are flat, they show a time difference sufficient to degrade the quality of stacking. This difference, caused by the 30°-dip of the intermediate interface (i.e., by lateral heterogeneity), is the reason for destructive intereference on time-migration stacks often observed in multi-azimuth time imaging.

For isotropic media, conventional processing leads to distortions when the overburden is laterally heterogeneous and the image point is located outside the incidence (sagittal) plane. The presence of heterogeneity requires application of an azimuthally-dependent migration operator, while out-of-plane image rays correspond to azimuthal imaging angles (i.e., the angles between the x-axis and the lines from the source/receiver positions to the emergence point of the image ray) different from the source-receiver azimuth. In our simple example, the image rays for reflections recorded on the strike line deviate from the incidence plane, which distorts the migration result obtained using a single best-fit velocity.

Next, the same image gathers in dip and strike directions were computed by our multi-azimuth prestack time migration, which takes the azimuthal velocity variation into account (Figure 4). After application of the optimal migration-velocity ellipse, flat gathers from different azimuthal directions are recorded at the same time and can be stacked to obtain a high-quality final image.

We also tested our algorithm on a laterally homogeneous azimuthally anisotropic model that includes an HTI layer sandwiched between two isotropic layers. The parameter $\delta^{(V)}$, which determines the elongation of the P-wave NMO ellipse in HTI media (Tsvankin, 1997), was intentionally chosen to be uncommonly large by absolute value. The synthetic data were generated with anisotropic ray tracing code ANRAY developed by Gajewski & Pšenčík (1987). Figure 5 shows several input common-offset, common-azimuth sections for the reflection from the bottom of the HTI layer.

The substantial time difference between the reflections in the planes parallel and perpendicular to the symmetry axis is caused by the pronounced azimuthal anisotropy (here associated with the parameter $\delta^{(V)}$). This difference would result in a significant imaging mismatch after conventional time migration, if a single velocity is used for both principal azimuthal directions. Note that image rays excited in either vertical symmetry plane of the HTI layer do not deviate from the incidence plane. Therefore, for this model it is possible to avoid the mismatch by migrating narrow-azimuth data for each symmetry plane with the best-fit velocity estimated for that plane by the conventional algorithm (i.e., the approach that failed for the isotropic model discussed above).

To carry out multi-azimuth time-migration velocity analysis, we used equation 12. The time-migration velocity ellipse was estimated by flattening the common-image gathers for the available offsets and azimuths. Because the symmetry-axis orientation is assumed to be known, velocity analysis has to be applied only in the principal directions of the model. The time-migrated images of the azimuth-offset sections from Figure 5 are displayed in Figure 6. Clearly, the reflection from the bottom of the HTI layer is imaged at the same position using all azimuth-offset combinations in the input data. Figure 7 shows the time-migration response of one of the constant-azimuth, constant-offset volumes in the form of a time-slice, as well as in-line and cross-line sections.

4 CONCLUSIONS

We introduced a method for multi-azimuth prestack time migration (MAPSTM) based on the azimuthally-dependent diffraction time function. Hamilton's principal equation helped to obtain a relationship between azimuthally varying time-migration velocities and 3D prestack time-migration operators for arbitrarily anisotropic, weakly heterogeneous media. The current version of the method employs a second-order traveltime approximation, which makes the MAPSTM operator sufficiently accurate only for small- and moderate-offset data. The operator depends on three independent parameters that form the "time-migration velocity ellipse." The ellipse is obtained from time-migrated multi-azimuth data by flattening common-image gathers for all available offsets and azimuths. In contrast to existing migration methods for azimuthally anisotropic (e.g., orthorhombic) media, our algorithm does not require estimation of the normal-moveout velocities and relevant anisotropy parameters.

To compare MAPSTM with conventional processing, we generated multi-azimuth synthetic data for two models, one of which is isotropic but laterally heterogeneous (it contains a dipping interface), while the other includes an HTI layer with strong azimuthal anisotropy. Although conventional migration may produce flat gathers in the principal azimuthal directions, the time of migrated events varies with azimuth. This time difference is sufficient to cause destructive intereference on time-migration stacks often observed in multi-azimuth time imaging. The time mismatch problem was fully resolved for both models by applying MAPSTM with the best-fit time-migration velocity ellipse.

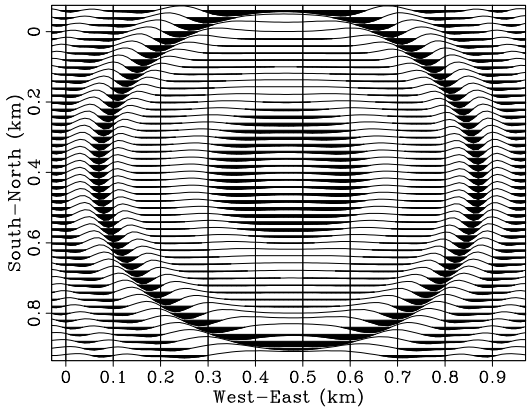

Figure 1. Time slice of the multi-azimuth time-migration operator.

ACKNOWLEDGMENTS

W. Söllner is grateful to PGS for permission to publish this work and to his colleagues B. Tsimelzon, S. Lee, and C. Gerrard for their help with an early version of this development. We thank the faculty and students of the Center for Wave Phenomena (CWP) for stimulating discussions. This work was partially supported by the Consortium Project on Seismic Inverse Methods for Complex Structures, CWP.

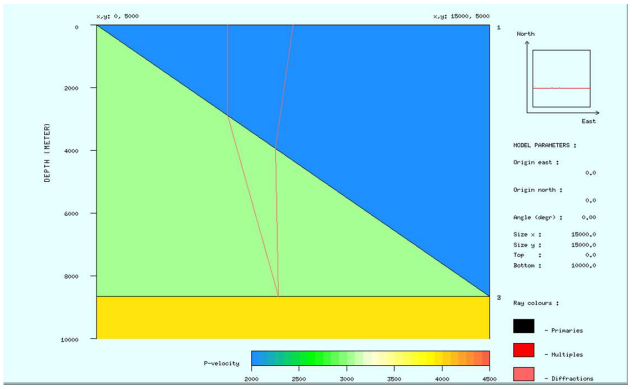

(a)

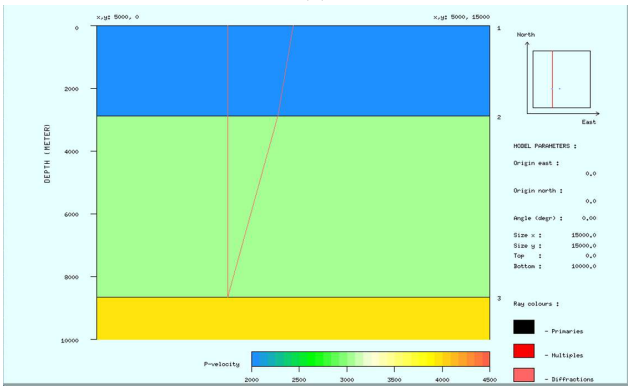

(b)

Figure 2. Dip (a) and strike (b) sections of the isotropic velocity model. An image ray at x=5 km and y=5.025 km (the position of the image gathers in Figures 3 and 4) is displayed along with two rays recorded at an offset of 2.5 km in the dip and strike directions.

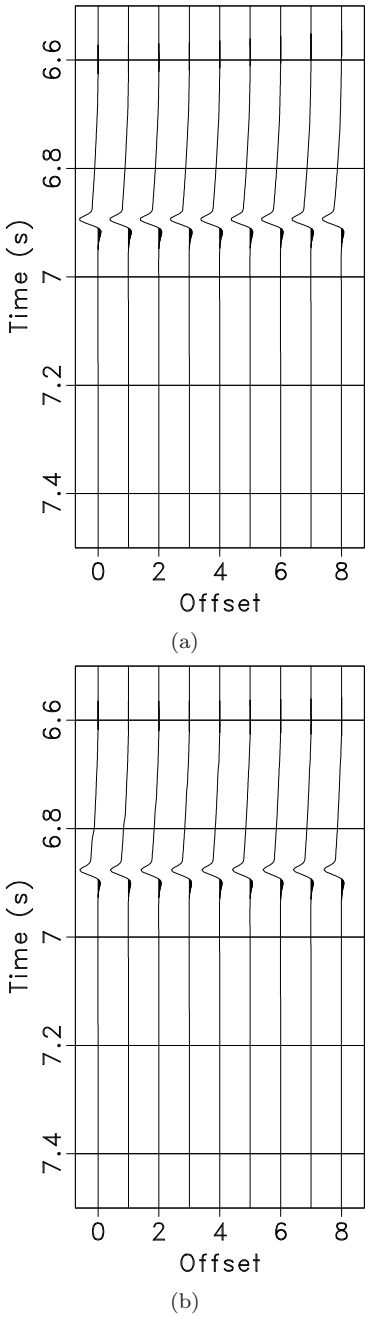

Figure 3. Conventional CIG gathers in the dip (a) and strike (b) directions for the isotropic model from Figure 2. The gathers are computed with the optimal migration velocity for each direction.

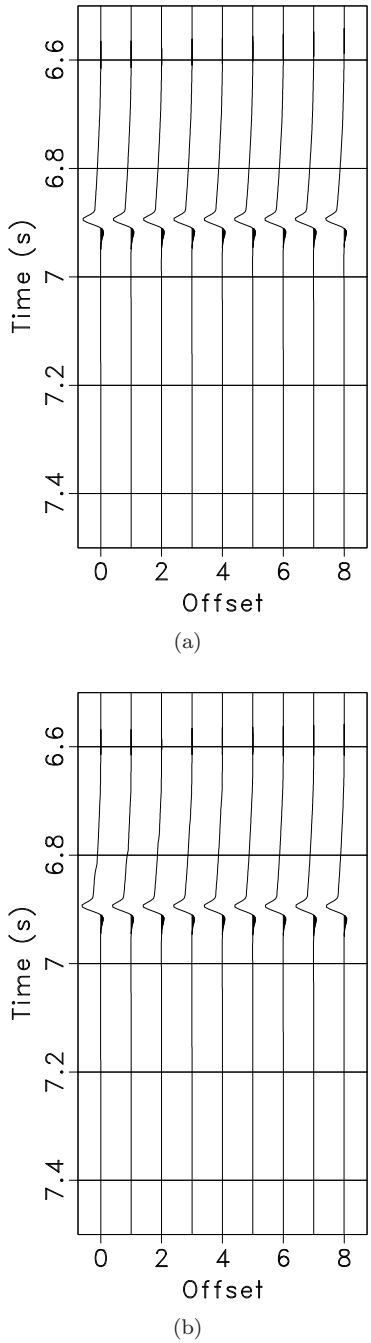

Figure 4. Multi-azimuth CIG gathers in the dip (a) and strike (b) directions for the isotropic model from Figure 2. Both gathers are computed with the optimal migration-velocity ellipse. The first offset and the offset increment in the CIG are 400 m.

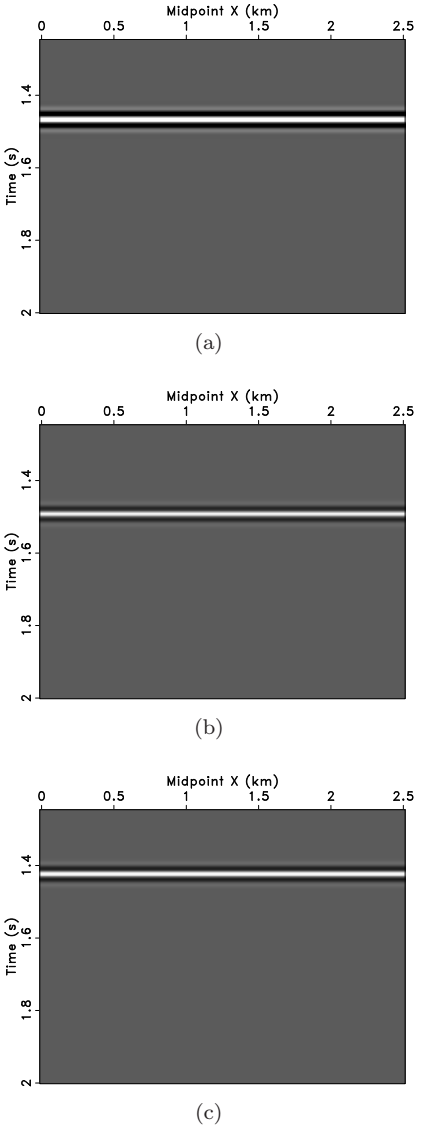

Figure 5. Input common-offset, common-azimuth sections for a model composed of three horizontal layers. The top and bottom layers are isotropic with the same velocity V_p=2.5 km/s; the intermediate (second) layer is HTI with $V_{P,\mathrm{vert}}$=3.25 km/s, $\delta^{(V)} = -0.348$, and $\epsilon = 0.4$. The azimuth and offset are 90° and 1000 m (a); 0° and 1000 m (b); and 0° and 100 m (c).

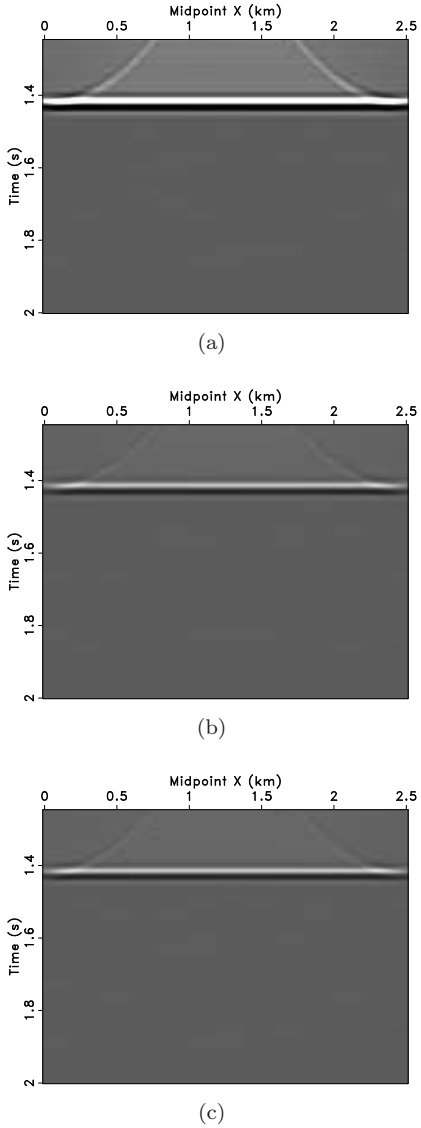

Figure 6. Time-migrated common-offset, common-azimuth sections generated by our multi-azimuth algorithm. The azimuth and offset are 90° and 1000 m (a); 0° and 1000 m (b); and 0° and 100 m (c).

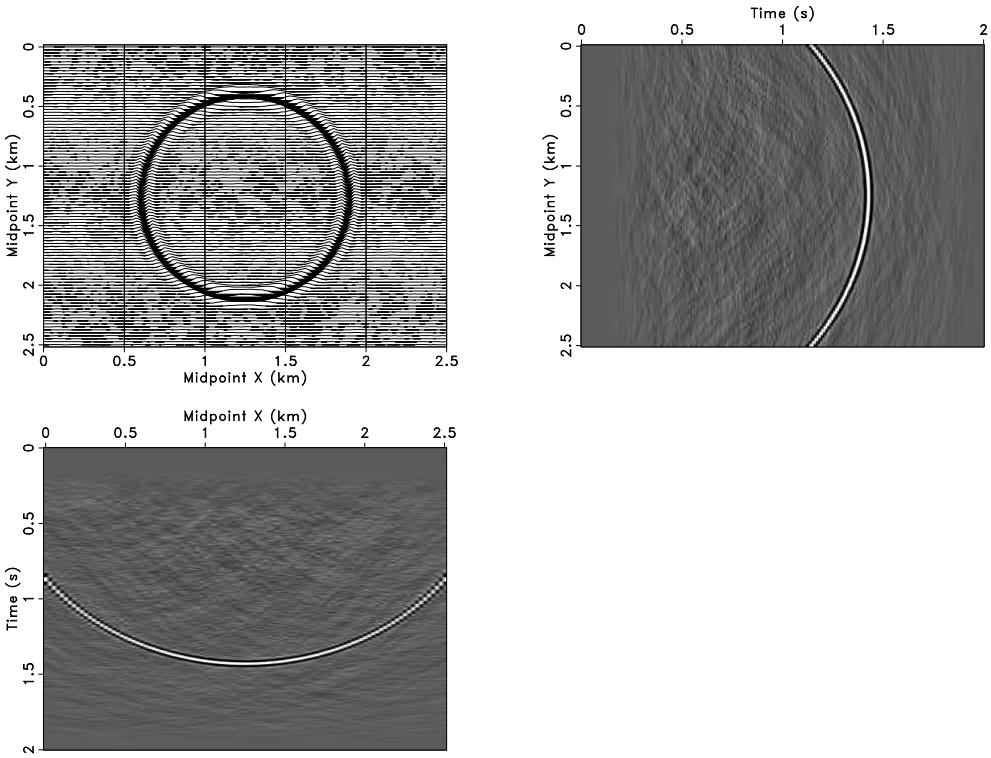

Figure 7. Multi-azimuth time-migration response for the input data with the azimuth 90° and offset 1000 m. The time slice at 1.3 s (top left); the inline section at y=1.25 km (top right); and the cross-line section at x=1.25 km (bottom).

References

Bortfeld, R. 1989. Geometrical ray theory: Rays and traveltimes in seismic systems (second-order approximations of the traveltimes). *Geophysics*, **54**(03), 342–349.

Buchdahl, H. 1970. *An introduction to Hamiltonian optics*. Cambridge University Press.

Calvert, A., Jenner, E., Jefferson, R. R., Bloor, R., Adams, N., Ramkhelawan, R., & St.Clair, C. 2008. Measuring and correcting for azimuthal anisotropy using Offset Vector Tile migration. *Geophysics*.

Červený, V. 2001. *Seismic ray theory*. Cambridge University Press.

Gajewski, D., & Pšenčík, I. 1987. Computation of high frequency seismic wavefields in 3-D laterally inhomogeneous anisotropic media. *geophysical Journal of the Royal Astronomical Society*, **91**, 383–412.

Grechka, V., & Tsvankin, I. 1998. 3-D description of normal moveout in anisotropic inhomogeneous media. *Geophysics*, **63**, 1079–1092.

Grechka, V., & Tsvankin, I. 1999. 3-D moveout velocity analysis and parameter estimation for orthorhombic media. *Geophysics*, **64**(3), 820–837.

Grechka, V., Helbig, K., & Pšenčík, I. 2006. The Eleventh International Workshop on Seismic Anisotropy (11IWSA). *Geophysics*, **71**(1), 13JF–29JF.

Hubral, P., & Krey, T. 1980. *Interval velocities from seismic reflection time measurements*. Society of Exploration Geophysicists.

Hubral, P., Schleicher, J., & Tygel, M. 1992. Three-dimensional paraxial ray properties - Part I. Basic relations. *Journal of Seismic Exploration*, **1**, 265–279.

Jäger, R., Mann, J., Höcht, G., & Hubral, P. 2001. Common reflection surface stack: Image and attributes. *Geophysics*, **66**, 907–109.

Keggin, J., Benson, M., Rietveld, W., Manning, T., Barley, B., Cook, P., Jones, E., Widmaier, M., Wolden, T., & Page, C. 2007. Multi-azimuth towed streamer 3D seismic in the Nile Delta, Egypt. *Pages 2891–2894 of: 76th Annual International Meeting, Expanded Abstracts*. SEG.

Manning, T., Shane, N., Page, C., Barley, B., Rietveld, W., & Keggin, J. 2007. Quantifying and increasing the value of multi-azimuth seismic. *The Leading Edge*, **26**, 510–520.

Moser, T. J., & Červený, V. 2007. Paraxial ray methods for anisotropic inhomogeneous media. *Geophysical Prospecting*, **55**, 21–37.

Schleicher, J., Tygel, M., & Hubral, P. 1993. Parabolic and hyperbolic paraxial two-point traveltimes in 3D media. *Geophysical Prospecting*, **41**, 495–513.

Schleicher, J., Tygel, M., & Hubral, P. 2007. *Seismic true-amplitude imaging*. Society of Exploration Geophysicists.

Söllner, W., & Andersen, E. 2005. Kinematic time migration and demigration in a 3D visualization system. *Journal of Seismic Exploration*, **15**, 255–270.

Tsvankin, I. 1997. Reflection moveout and parameter estimation for horizontally transverse isotropy. *Geophysics*, **62**, 614–629.

Tsvankin, I. 2005. *Seismic signatures and analysis of reflection data in anisotropic media*. Elsevier Science Publ. Co., Inc.

Vasconcelos, I., & Tsvankin, I. 2006. Nonhyperbolic moveout inversion of wide-azimuth P-wave data for orthorhombic media. *Geophysical Prospecting*, **54**, 535–552.

APPENDIX A: REFLECTED RAYS AND NMO-VELOCITY EQUATION

Here, we consider the same model as in the main text, but the normal ray will be treated as the central ray. By definition, the final slowness vector of the normal ray vanishes: $\mathbf{p'}_0 = \mathbf{0}$. Hamilton's point characteristic for reflected rays is obtained by treating a reflected ray as the combination of the two downgoing transmitted rays, which obey Snell's law at the reflection point (Bortfeld, 1989; Hubral *et al.*, 1992):

$$\begin{aligned} T(\mathbf{x}_r,\mathbf{x}_s) =& T_0 - 2\mathbf{p}_0\cdot\frac{1}{2}(\mathbf{x}_r+\mathbf{x}_s) \\ &+ \frac{1}{2}(\mathbf{x}_r+\mathbf{x}_s)\cdot\mathbf{D}_0^{-1}\,\mathbf{C}_0\frac{1}{2}(\mathbf{x}_r+\mathbf{x}_s) \\ &+ \frac{1}{2}(\mathbf{x}_r-\mathbf{x}_s)\cdot\mathbf{B}_0^{-1}\mathbf{A}_0\,\frac{1}{2}(\mathbf{x}_r-\mathbf{x}_s)\,, \end{aligned} \quad \text{(A1)}$$

where T_0 is the exact two-way traveltime along the normal ray with the source and receiver positions $\mathbf{x}_s = \mathbf{x}_r = \mathbf{0}$. Equation A1 gives the reflection traveltimes of reflected rays from any source position $\mathbf{x}_s$ to any receiver position $\mathbf{x}_r$ in the second-order approximation. The 2×2 symmetric surface-to-surface matrix combinations $\mathbf{B}_0^{-1}\mathbf{A}_0$ and $\mathbf{D}_0^{-1}\mathbf{C}_0$ are related to the NIP and normal wavefront, respectively (Hubral & Krey, 1980). The hyperbolic reflection time function is obtained by squaring both sides of equation A1 and keeping terms up to the second order (Schleicher *et al.*, 1993):

$$\begin{aligned} T^2(\mathbf{x}_r,\mathbf{x}_s) =& [T_0 - 2\mathbf{p}_0\cdot\frac{1}{2}(\mathbf{x}_r+\mathbf{x}_s)]^2 \\ &+ 2T_0\frac{1}{2}(\mathbf{x}_r+\mathbf{x}_s)\cdot\mathbf{D}_0^{-1}\mathbf{C}_0\frac{1}{2}(\mathbf{x}_r+\mathbf{x}_s) \\ &+ 2T_0\frac{1}{2}(\mathbf{x}_r-\mathbf{x}_s)\cdot\mathbf{B}_0^{-1}\mathbf{A}_0\frac{1}{2}(\mathbf{x}_r-\mathbf{x}_s). \end{aligned} \quad \text{(A2)}$$

Equation A2 has found a wide range of applications (Jäger *et al.*, 2001).

The reflection time function for a CMP gather with

the midpoint at the origin of the coordinate system is obtained from equation A2 by setting $\frac{1}{2}(\mathbf{x}_r + \mathbf{x}_s)$=**0**:

$$T^2(\mathbf{x}_r, \mathbf{x}_s) = T_0^2 + 2T_0 \frac{1}{2}(\mathbf{x}_r - \mathbf{x}_s) \cdot \mathbf{B}_0^{-1}\mathbf{A}_0 \frac{1}{2}(\mathbf{x}_r - \mathbf{x}_s). \quad \text{(A3)}$$

We denote the three independent elements of the symmetric 2×2 matrix $\mathbf{B}_0^{-1}\mathbf{A}_0$ by W_{11}, W_{12}, W_{22}, and express the offset vector $\mathbf{x}_r - \mathbf{x}_s$ through its magnitude h and angle α with the x-axis. After carrying out the vector-matrix operations, equation A3 becomes:

$$T^2(\mathbf{x}_r, \mathbf{x}_s) = T_0^2 + \frac{T_0}{2}(W_{11}\cos^2\alpha + 2W_{12}\cos\alpha\sin\alpha + W_{22}\sin^2\alpha)\, h^2 = T_0^2 + \frac{h^2}{V_{\rm nmo}^2(\alpha)}, \quad \text{(A4)}$$

where

$$V_{\rm nmo}^{-2}(\alpha) = \frac{T_0}{2}(W_{11}\cos^2\alpha + 2W_{12}\cos\alpha\sin\alpha + W_{22}\sin^2\alpha). \quad \text{(A5)}$$

Equations A4 and A5 are equivalent to the equation of the NMO ellipse derived by Grechka & Tsvankin (1998). The parameters W_{11}, W_{12}, and W_{22} of the global matrix combination $\mathbf{B}_0^{-1}\mathbf{A}_0$ define the NMO ellipse and can be estimated from hyperbolic moveout analysis for at least three distinct azimuths of the CMP line. The NMO-velocity equations A4 and A5 appear to be similar to equations 10 and 11 for the azimuthally-varying time-migration velocity. However, NMO and time-migration velocities are identical only in the special case when the normal and image rays coincide, which happens in horizontally layered media. In order to derive a time-migration operator from NMO velocities (around the normal ray), it will be necessary to add dip information.

A1 Time migration based on NMO velocities

To develop a time-migration formalism using the normal ray and NMO velocities, we use an approach different from the one described in the main text. As before, we consider the diffraction time function of a hypothetical diffractor at the reflection point. But here we start from the normal ray (instead of the image ray) treating every time sample along the normal ray as a possible reflection point and stacking along the corresponding diffraction time function. The stacked amplitude value is assigned to the image time (two-way traveltime along the image ray). The image ray is the transmitted ray between the earth's surface and the reflection point, whose initial slowness vector is perpendicular to the surface. If no reflector is found at the endpoint of the normal ray, the amplitude obtained by summation is expected to vanish.

The diffraction time function of a diffractor at the endpoint ($\mathbf{x}' = \mathbf{0}$ and $\mathbf{p}'_0 = \mathbf{0}$) of the normal ray (in this case chosen as the central ray) is obtained from Hamilton's point characteristic in equation 7. For example, the traveltime from the receiver $\mathbf{x}_r$ to the diffraction point is

$$t(\mathbf{x}_r, \mathbf{x}' = \mathbf{0}) = t_0 - \mathbf{p}_0 \cdot \mathbf{x}_r + \frac{1}{2}\mathbf{x}_r \cdot \mathbf{B}_0^{-1}\mathbf{A}_0\,\mathbf{x}_r\,, \quad \text{(A6)}$$

where t_0 is the exact one-way traveltime along the central ray; the initial slowness vector $\mathbf{p}_0$ and the product $\mathbf{B}_0^{-1}\mathbf{A}_0$ also correspond to that ray. The second-order (hyperbolic) approximation is obtained by squaring both sides of equation A6 and dropping third- and higher-order terms:

$$t^2(\mathbf{x}_r, \mathbf{x}' = \mathbf{0}) = [t_0 - \mathbf{p}_0 \cdot \mathbf{x}_r]^2 + t_0\,\mathbf{x}_r \cdot \mathbf{B}_0^{-1}\mathbf{A}_0\,\mathbf{x}_r\,. \quad \text{(A7)}$$

The three independent elements W_{11}, W_{12}, W_{22} of the 2×2 symmetric matrix $\mathbf{B}_0^{-1}\mathbf{A}_0$ can be found from azimuthal moveout analysis, as discussed above (equations A4 and A5). Finally, the diffraction time function is obtained by substituting the NMO ellipse into equation A7 and adding a similar traveltime term for the transmitted ray from the source position $\mathbf{x}_s$:

$$T_D = \sqrt{[t_0 - \mathbf{p}_0 \cdot \mathbf{x}_r]^2 + \frac{l_r^2}{V_{\rm nmo}^2(\phi)}} + \sqrt{[t_0 - \mathbf{p}_0 \cdot \mathbf{x}_s]^2 + \frac{l_s^2}{V_{\rm nmo}^2(\gamma)}}. \quad \text{(A8)}$$

The distances l_r and l_s are measured from the normal ray (where the NMO ellipse is determined), and γ and ϕ are the azimuths to the source and receiver, respectively. Given the NMO ellipse and the initial slowness vector of the central ray, equation A8 yields the diffraction times for any source-receiver combination in the prestack data. The final image time and image position are found by simply searching for the shortest two-way time among all rays transmitted from the surface to the diffraction point.

Equation A8 helps us understand the difference between the two time-migration approaches discussed here. Whereas the algorithm based on the image-ray parameters (equation 12) requires only the time-migration velocities, time migration operating with the normal-ray parameters (equation A8) needs not just the NMO ellipse but also the initial slowness vector $\mathbf{p}_0$ (i.e., the horizontal slowness) of the normal ray. However, with the vector $\mathbf{p}_0$ estimated from zero-offset time slopes, the two approaches produce equivalent time-migration operators (in the second-order approximation). A post-stack version of time migration based on NMO velocities and zero-offset slopes is used in Söllner & Andersen (2005) for 3D kinematic imaging.